

Lateral Guidance & Control Design for an Unmanned Aerial Vehicle

Raza Samar Shakil Ahmed Muhammad Nzar

*Centre for Control & Instrumentation,
National Engineering & Scientific Commission, Islamabad, Pakistan
(e-mail of first author: raza@mail.comsats.net.pk).*

Abstract: This paper presents guidance and control design for a UAV, and its six degrees-of-freedom nonlinear simulation results. The paper focuses on the lateral control and guidance aspects; longitudinal control aspects will be addressed separately in another paper. An introduction to the lateral mission, and guidance problem is given first. Waypoints for straight and turning flight paths are defined. Computation of various flight path parameters is discussed, including formulae for down-range (distance travelled along the desired track), cross-track deviation and heading error of the vehicle; these are then used in the lateral guidance algorithm. The lateral guidance law is then presented, followed by the design of a multivariable H_∞ controller for roll control and stability augmentation. The controller uses the ailerons and rudder for control. The reference roll angle is provided by the guidance law. The sensors available on-board the vehicle do not measure yaw-rate, hence a practical method of its estimation is proposed. The entire guidance and control scheme is implemented on a full nonlinear six degrees-of-freedom simulation of the vehicle. Simulation results are presented and discussed.

Keywords: Guidance and control of vehicles; Trajectory tracking and path following; Robust control applications.

1. INTRODUCTION

Successful control system design for high performance UAVs requires efficient and effective techniques for the design of guidance and control algorithms that ensure satisfactory operation in the face of system uncertainties. In this paper, we develop and present one such technique. The UAV under consideration is a high performance vehicle, shown in Fig. 1. It is propeller driven in a push configuration. Pitch control is provided by a set of canards located forward of the main wing, roll control is provided by ailerons on the main wing, and the two vertical tails have rudders. The cruising speed is about 60 m/sec. The main tasks of the guidance and control system are to:

- fly the vehicle on the desired mission path, with minimum cross-track deviation,
- make decisions about various flight events, such as achievement of waypoints, and
- provide robust stabilization during flight.

This paper is organized as follows. Section 2 describes the mission plan on which we intend the UAV to fly, while section 3 formulates the guidance and control problem in specific terms. Section 4 develops the basic formulae used for flight path computation. These form the basis for taking real-time decisions during flight and for implementing the guidance law. The nonlinear guidance law is discussed in section 5. Section 6 describes the design of the robust multivariable H_∞ controller and discusses robustness of the controller across the flight envelope. Simulation results are presented and discussed in section 7; section 8 concludes the paper.



Fig. 1. A photograph of the experimental UAV.

2. THE MISSION PLAN

The mission of the UAV is planned in advance and loaded into the Flight Control Computer before flight. The mission plan consists of a number of waypoints which define the path the UAV is going to take. The entire mission can be represented by a series interconnection of straight line segments, arcs and circles (for loiter). Fig. 2

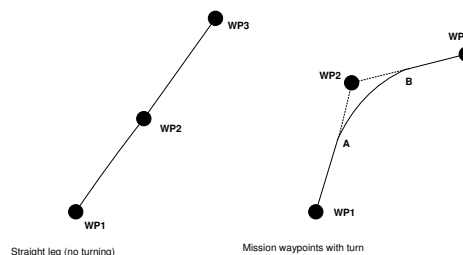


Fig. 2. Waypoints for straight and turning flight.

shows on the left hand side part of a mission comprising of a straight line segment. In this case the UAV is required to fly through the waypoint $WP2$. The right side of Fig. 2 shows part of a mission with a turn. Here the UAV is not required to go through the central waypoint ($WP2$) but rather fly on a circular arc AB close to $WP2$. Point A is where the turn starts and B is where it ends. Similarly loiter missions are also possible where the vehicle flies in a circular orbit around a given waypoint. Here we shall assume that a mission has been planned and the mission data in terms of waypoints is available to the Flight Control Computer.

3. PROBLEM FORMULATION

We now formulate the problem in more specific terms. The task of the lateral guidance and control system is defined as to:

- Compute the down-range covered, and the cross-track deviation from the designated track/trajectory,
- Compute the error in heading angle of the vehicle,
- Determine if a waypoint is achieved,
- Compute 'turn start' and 'turn stop' decision flags for the autopilot,
- Solve the guidance equations to calculate the roll reference command for steering the vehicle back onto the desired path, and
- Control the lateral-directional dynamics of the vehicle throughout the flight envelope in the presence of disturbances.

All the above computations have to be done in real time. The available control inputs to the vehicle are the ailerons and the rudder. Note that the cross-track deviation and heading error are used in the guidance equations.

4. FLIGHT PATH COMPUTATIONS

Here we present the basic flight path computations that are performed in real time to enable navigation of the vehicle through a sequence of straight and turning waypoints. Waypoints are defined as geographic positions in terms of latitude and longitude. For any three consecutive waypoints $WP1$, $WP2$ and $WP3$, if the turn angle (defined as the difference of azimuths of $WP1$ and $WP3$ at $WP2$) at the central waypoint ($WP2$) is nearly 180° , then the path from $WP1$ to $WP2$ will be considered a straight line, and $WP2$ will be referred to as a *straight* waypoint. On the other hand if the turn angle is significant, then $WP2$ will be referred to as a *turning* waypoint and the path from $WP1$ to $WP3$ will consist of straight and curved parts (Fig. 2). Flight path computations are worked out for both straight and curved paths; however only straight path formulae will be presented here due to space limitation.

Let $WP1(\phi_1, \lambda_1)$, $WP2(\phi_2, \lambda_2)$ and $WP3(\phi_3, \lambda_3)$ be three consecutive waypoints (ϕ and λ denote the latitude and longitude, respectively), and let $M(\phi_M, \lambda_M)$ be the current position of the vehicle. We define an Earth-Centred Earth-Fixed (ECEF) frame with its origin at the centre of mass of the earth, the z-axis directed north along the polar axis, the x-axis in the equatorial plane and passing through the Greenwich Meridian, and the y-axis also in the equatorial plane and passing through 90° east longitude.

The position vector of a point on the earth's surface with latitude ϕ and longitude λ in ECEF frame is given by:

$$r_x = a \cos \phi_r \cos \lambda, \quad r_y = a \cos \phi_r \sin \lambda, \quad r_z = b \sin \phi_r \quad (1)$$

where a is the equatorial radius, b is the polar radius, and $\phi_r = \tan^{-1}(\frac{b}{a} \tan \phi)$ is the reduced latitude of the point under consideration. Let \vec{r}_1 and \vec{r}_2 be the position vectors of $WP1$ and $WP2$ in ECEF frame, respectively. The distance between $WP1$ and $WP2$ can be calculated as:

$$r_{12} = \frac{1}{2}(|\vec{r}_1| + |\vec{r}_2|) \cos^{-1}(\hat{r}_1 \cdot \hat{r}_2),$$

where \hat{r} is a unit vector along \vec{r} .

Cross-track deviation Cross-track error is the normal instantaneous displacement of the vehicle from the desired track. To compute the cross-track error we first define a vector \vec{r}_N normal to the trajectory plane (plane containing $WP1$, $WP2$ and the centre of the earth) as:

$$\vec{r}_N = \hat{r}_1 \times \hat{r}_2.$$

If \vec{r}_M is the position vector of the vehicle in ECEF frame, then the cross-track error will be $-\vec{r}_M \cdot \hat{r}_N$.

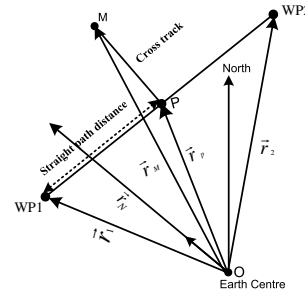


Fig. 3. Straight flight path definitions.

Heading error If V_E denotes the east velocity and V_N the north velocity of the vehicle, then the velocity heading of the vehicle is given by $\psi_G = \tan^{-1}(\frac{V_E}{V_N})$. Heading error is the difference between the actual velocity heading ψ_G and the desired heading ψ_R , i.e., $\psi_E = \psi_G - \psi_R$. If P is the projection of the vehicle's current position on the trajectory plane, then the desired heading angle (ψ_R) is the angle between the trajectory plane and the meridian plane passing through the projected point P . The position vector \vec{r}_P of the projected point P in ECEF frame is given by:

$$\vec{r}_P = \vec{r}_M - (\vec{r}_M \cdot \hat{r}_N) \hat{r}_N.$$

The desired heading angle ψ_R works out to be:

$$\psi_R = \tan^{-1} \left[\frac{|\hat{r}_P \times \hat{k}| \cdot \hat{r}_N}{(\hat{r}_P \times \hat{k}) \cdot \hat{r}_N} \right], \quad (2)$$

where \hat{k} is a unit vector along the earth's spin axis.

Waypoint achieved criterion The straight waypoint $WP2$ is achieved, when the straight path distance covered exceeds r_{12} . The straight distance covered from $WP1$ to the current position of the vehicle is $\frac{1}{2}(|\vec{r}_1| + |\vec{r}_P|) \cos^{-1}(\hat{r}_1 \cdot \hat{r}_P)$.

5. LATERAL GUIDANCE LOGIC

The block diagram of the lateral/directional guidance and control system is shown in Fig. 4. The outputs of the UAV that are measured by on-board sensors include the attitude angles, i.e., roll, pitch (measured by a vertical gyro) and heading (measured by a magnetic sensor) and the (GPS) position and velocity of the vehicle. The outer loop is the lateral guidance loop that looks at the measured position and velocity of the vehicle, compares it with the desired mission path, and generates a roll reference command that acts as a reference for the inner loop to follow. The inner loop has roll and yaw-rate feedbacks; the yaw-rate is computed from the attitude angles as discussed in §6.1 below. The lateral guidance scheme used is based on the work by Park et al. [2004]. The basic scheme is modified by introducing an adaptive tuning of the reference length to enhance the performance for large cross-track errors. Integral action is also added to improve tracking in the presence of constant disturbances. Here we will mainly discuss the proposed modifications in the basic scheme (Fig. 5). In the figure C is the vehicle's instantaneous

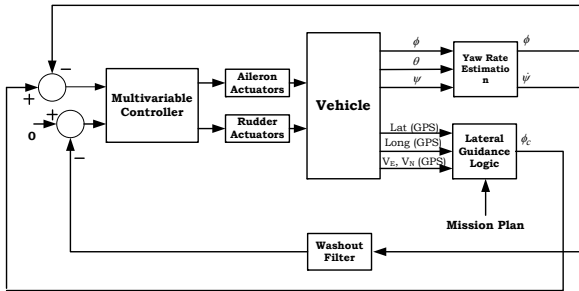


Fig. 4. Block diagram of the guidance and control system.

position, D is a reference point selected on the desired path AB , L_1 is the length of the line CD , V is the velocity of the vehicle, and η is the angle between the velocity vector and CD . The roll command ϕ_c generated by the basic scheme is given as:

$$\phi_c = \tan^{-1} \left[\frac{2V^2}{gL_1} \sin \left\{ \sin^{-1} \left(\frac{y}{L_1} \right) + \psi_E \right\} \right], \quad (3)$$

where y is the instantaneous cross-track deviation, ψ_E is the heading error, and g is the acceleration due to gravity. Guidelines for selection of the length L_1 are given by Park et al. [2004] in which (3) is linearized to yield a second

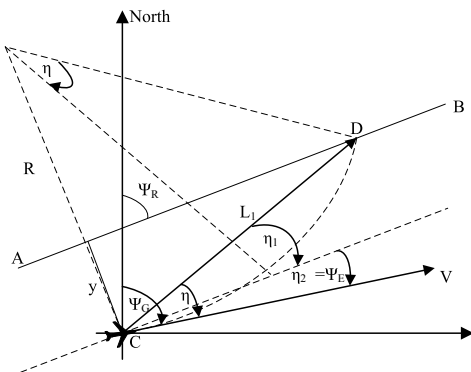


Fig. 5. Nonlinear guidance logic setup.

order system with $\zeta = 1/\sqrt{2}$, $\omega_n = \sqrt{2}V/L_1$, where ζ and ω_n refer to the damping ratio and natural frequency of the standard second order system.

5.1 Adaptive tuning of length L_1

For system stability it is required that $y < L_1$ and $|\eta| < \pi/2$ (Park et al. [2004]). However, for UAVs there is always a possibility of developing large cross-track errors. This could be due to the runway not being in the direction of the first waypoint, or the GPS signal becoming unavailable for an extended period during flight. In such cases, the condition $y < L_1$ may not be satisfied (for a relatively small and fixed L_1) making ϕ_c undefined. Also selection of L_1 determines the speed of response. If a fast response is desired, a small L_1 may be selected, leading to large roll angles bringing the vehicle back on the desired path quickly (with possibly high overshoots). A larger L_1 will make the system slower and reduce overshoot. This is discussed by Samar et al. [2007] with reference to gain selection for a conventional proportional-derivative guidance law where the gains are scheduled with the magnitude of the cross-track error. It may be noted here that to cater for large cross-track errors, L_1 will have to be kept unduly large which may yield poor performance otherwise. On the other hand if a relatively smaller L_1 is selected, the resulting roll angle might become too large and exceed the set limit. A simple solution for this problem is to introduce an adaptive adjustment of L_1 with cross-track error. We define a compensated reference length \hat{L}_1 to be used in (3) instead of a fixed L_1 :

$$\hat{L}_1 = L_1 + k_1|y|, \quad (4)$$

where k_1 is a positive gain to be tuned, usually taken to be greater than 1 (a value of 1.5 for our application gave good results). Roll angle commands are computed using L_1 and \hat{L}_1 and compared (with $V = 50$ m/s, $L_1 = 350$ meters, and $\psi_E = 10$ deg) in Table 1. The table shows

Cross-track (m)	ϕ_c (deg) using L_1	ϕ_c (deg) using \hat{L}_1
45	24	19
90	32	20
175	43	20
350	55	18
700	Undefined	13

Table 1. ϕ_c computed using L_1 and \hat{L}_1 .

that for large cross-track errors, the roll angle command computed using \hat{L}_1 remains reasonably small, and can be designed to lie within a suitable range.

5.2 Addition of integral action

Roll angle command as given in (3) is modified by addition of an integrator for strict path tracking in the presence of constant wind disturbances. Addition of an integrator in the loop can pose problems such as wind-up leading to control surface saturation, for which the following actions may be taken:

- integral action may be activated only when the cross-track error becomes smaller than a certain threshold, and

- the integrator state may be limited to a pre-defined value; the integrator may be switched off if its state exceeds the set limit.

With the addition of integral action, and using \hat{L}_1 instead of L_1 , (3) becomes:

$$\phi_c = \tan^{-1} \left[\frac{2V^2}{g\hat{L}_1} \sin \left\{ \sin^{-1} \left(\frac{y}{\hat{L}_1} \right) + \psi_E \right\} \right] + k_2 \int \hat{y} dt \quad (5)$$

where the integral gain k_2 is tuned by simulation, $\hat{y} = \begin{cases} y & \text{if } y \leq y_{th} \\ 0 & \text{if } y > y_{th} \end{cases}$, and $y_{th} = 100$ m.

6. ROBUST MULTIVARIABLE CONTROLLER DESIGN

For controller design, we use the H_∞ loop-shaping design procedure given by McFarlane and Glover [1992]. The procedure is intuitive in that it is based on the multivariable generalization of classical loop-shaping ideas. The open-loop plant, once given the desired loop-shape, is robustly stabilized against coprime factor uncertainty. The resulting controller has been shown to enjoy some favourable properties, such as no pole-zero cancellation occurs in the closed-loop system (except for a certain special class of plants), see Tsai et al. [1992]. In addition, the controllers thus designed have been successful in various applications; examples are those described in Samar et al. [1996], Smerlas et al. [2001], Postlethwaite et al. [2005], and Skogestad and Postlethwaite [2005].

6.1 The Plant Model

The lateral/directional control system is a multivariable control system as shown in Fig. 4. The roll and pitch angles are sensed by the vertical gyro which has very fast dynamics as compared to the vehicle, and so this sensor is modelled as a simple gain in the feedback loop. The magnetic sensor (which senses the heading angle) dynamics are also neglected. The actuator dynamics are modelled by 2^{nd} order transfer functions. The model of the UAV for controller design is taken as a linear approximation obtained at a cruise altitude of 2000 m and a speed of 60 m/sec. It may be noted that the flight envelope consists of an altitude range from 200–5000 m and a speed bracket from 40–70 m/sec. A number of linear models are available across the flight envelope to test the robustness of the control system at different operating conditions. Note that the final plant has 2 inputs and 2 outputs. The inputs are the aileron and rudder deflection commands to the actuators. The outputs are the roll angle and the filtered yaw-rate of the vehicle. The computation of the yaw-rate and its filtering is discussed below.

Yaw-rate computation Feedback of yaw-rate is considered useful for providing damping to the dutch roll mode of the vehicle. But the vertical gyro does not provide measurement of angular rates; it only measures roll and pitch angles. Body angular rates are computed from attitude angles as follows.

We define a navigation axis system ($X_n Y_n Z_n$) in which the Z_n axis is upwards along the local vertical, and the X_n and Y_n axes are in the local horizontal plane directed eastward

and northward, respectively. The (true) heading, pitch and roll angles are denoted by ψ , θ and ϕ respectively. The heading rotation occurs first about the Z_n axis, followed by the pitch rotation about the X'_n axis, finally followed by the roll rotation about the Y''_n axis to align the navigation axes with the body axes. Resolving the Euler angle rates $\dot{\psi}$, $\dot{\theta}$ and $\dot{\phi}$ into body axes, we can solve for the body axis rates. Denoting the roll, pitch and yaw rates in the body axes by P , Q and R respectively, we have:

$$\begin{aligned} P &= \dot{\psi} \sin \theta + \dot{\phi} \\ Q &= \dot{\theta} \cos \phi - \dot{\psi} \cos \theta \sin \phi \\ R &= \dot{\theta} \sin \phi + \dot{\psi} \cos \theta \cos \phi \end{aligned} \quad (6)$$

It may be noted that the attitude sensors measure the body angles and not their rates. The derivatives of the attitude angles are computed by fitting a least-squares line to four attitude measurements. If for example the pitch angle measurements from the vertical gyro are denoted by θ_0 , θ_1 , θ_2 and θ_3 , where θ_0 corresponds to the current measurement and θ_3 corresponds to the measurement taken three samples earlier, then the slope of the least squares line for these points approximates the derivative (Mathews [1992]):

$$\dot{\theta} \approx \frac{3\theta_0 + \theta_1 - \theta_2 - 3\theta_3}{10\Delta t} \quad (7)$$

This approximation of the derivative gives a good compromise between sensitivity to measurement noise and the delay introduced into the estimation of $\dot{\theta}$.

Washout filter Yaw-rate feedback is typically useful during transients, when the yaw-rate varies rapidly, or exhibits appreciable changes with time. The rudder is normally employed to suppress the yaw-rate oscillations to provide damping to the dutch roll mode of the vehicle. Thus during steady turns when there is a nearly constant yaw-rate, it is not desirable for the rudder to oppose the motion. The washout filter is a high pass filter that is used to feedback the yaw-rate at higher frequencies, effectively breaking the feedback at dc to enable steady turning of the vehicle. The washout filter is chosen as $W_w = \frac{s}{s+1}$; it may be thought of as a frequency-dependent weight on the yaw-rate output, with a low gain at low frequency (below 1 rad/sec), and unity gain at higher frequencies.

6.2 Controller design

Here we will describe the design of the lateral controller using the design procedure given by McFarlane and Glover [1992].

- (1) Singular values of the open-loop plant $G(s)$ are plotted and these indicate the need for boosting the low frequency gain for good tracking and disturbance rejection for the roll control channel. The low frequency gain is boosted by introducing integral action in the roll control loop; we choose to place a pole at $s = -0.01$ instead of using a pure integrator. The pre-compensator or weight W_1 is chosen as $\begin{bmatrix} \frac{28(s+2.5)}{s+0.01} & 0 \\ 0 & 40 \end{bmatrix}$ and the post-compensator

W_2 as $\begin{bmatrix} \frac{14(s+2)}{s+70} & 0 \\ 0 & \frac{50}{s+50} \end{bmatrix}$. Since we are aiming

for a closed-loop bandwidth of approximately 12–15 rad/sec, therefore zeros are introduced at -2.5 and -2 in W_1 and W_2 to reduce the roll-off at the cross-over frequency. The poles at -70 and -50 in W_2 are placed to provide adequate roll-off at higher frequencies. Since W_{11} (the upper left element of W_1) has an (approximate) integrator, it will be implemented in its conditioned form. Gains are selected in W_1 and W_2 to adjust the cross-over frequency to around 10 rad/sec.

The shaped plant $G_s = W_2GW_1$ is now formed, its singular values are shown in Fig. 6. The low frequency gain in the roll channel is boosted, as indicated by the larger singular value. The washout filter in the yaw-rate channel means that the low frequency gain in this channel remains low, as indicated by the smaller singular value of the shaped plant.

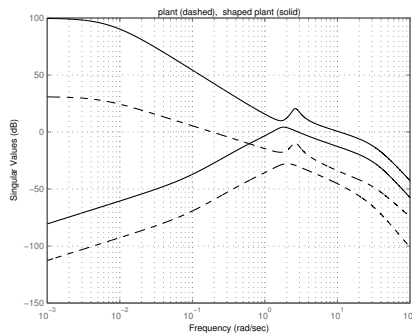


Fig. 6. Singular values of the original and shaped plants.

- (2) An optimal γ of 1.925 is computed; the controller is obtained for a slightly sub-optimal γ of 2.02.
- (3) The controller is reduced using optimal Hankel-norm approximation, and cascaded with the weights W_1 and W_2 , to form the complete controller W_1KW_2 . This reduced controller is discretized using the bilinear (Tustin's) approximation for implementation.

The singular values of the sensitivity function are shown in Fig. 7. One of the singular values, the one that remains flat at low frequencies, corresponds to yaw-rate and indicates no disturbance rejection on that output.

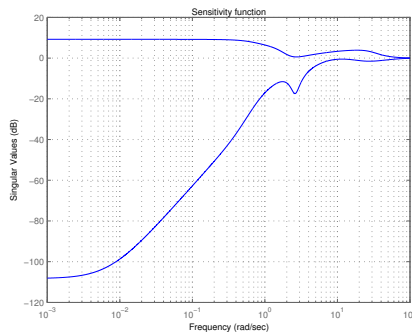


Fig. 7. Sensitivity function $(I + GW_1KW_2)^{-1}$.

6.3 Robustness analysis

Robust stability across the flight envelope is tested by obtaining normalized coprime factorizations of different plants in the envelope (a transfer matrix G is defined in terms of its normalized coprime factors \tilde{M} and \tilde{N} as $G = \tilde{M}^{-1}\tilde{N}$), and then taking their differences from the nominal plant to get uncertainty transfer functions $[\Delta_{\tilde{M}_i} \ \Delta_{\tilde{N}_i}]$, where the subscript i refers to the i^{th} plant of the envelope. Singular values of these uncertainty transfer functions are plotted in Fig. 8; the maximum of these across all frequencies equals 0.46. The γ for our controller is 2.02, which indicates that the robustness condition of McFarlane and Glover [1990], i.e.,

$$\|[\Delta_{\tilde{M}} \ \Delta_{\tilde{N}}]\|_{\infty} < \gamma^{-1}, \quad (8)$$

is satisfied, thus ensuring robust stability for the family of plants considered in the envelope.

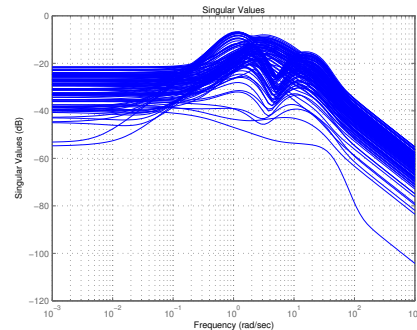


Fig. 8. Singular values of $[\Delta_{\tilde{M}} \ \Delta_{\tilde{N}}]$ for different plants.

7. NONLINEAR SIMULATION RESULTS

The complete guidance and control scheme is tested on a full nonlinear six degrees-of-freedom simulation of the vehicle for various missions and flight conditions. Part of a typical mission and its simulation results are presented here. Fig. 9 shows waypoints (small circles) joined by straight lines, and the actual path flown by the vehicle. The top half of Fig. 10 shows the wind disturbance used in the simulation. The bottom half shows the 'turn start/stop' flag (1 is for turn start, 0 is for turn stop) and the 'waypoint achieved' flag (the integer value of the flag depicts the number of the waypoint achieved). The cross-track error is small (less than 20 m) as shown in Fig. 11. Fig. 12 shows the commanded and actual roll angles, the commanded angle being generated by the guidance equation (5). The roll angle tracking provided by the multivariable controller is quite good. The bottom half of the figure shows the yaw-rate of the vehicle and the output of the washout filter. It is seen that the washout filter blocks the yaw-rate feedback during steady turns and only feeds through the high frequency transients. Actuator deflections (aileron (left and right) and rudder) are shown in Fig. 13.

8. CONCLUSIONS

A complete methodology for the design of lateral-directional guidance and control systems for high performance UAVs

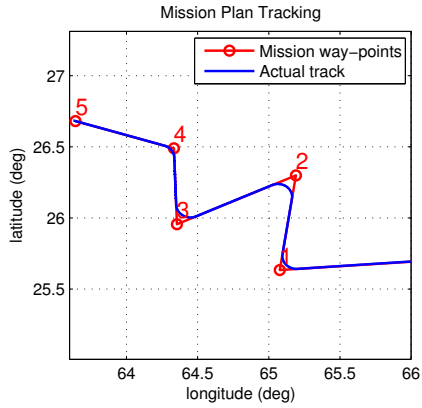


Fig. 9. Waypoints and the path flown by the vehicle.

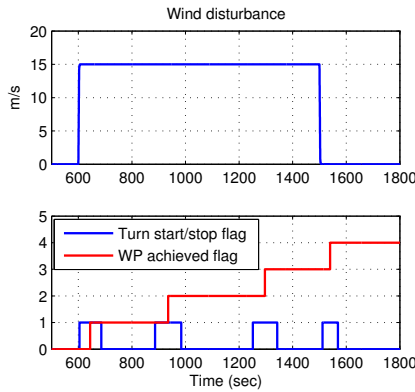


Fig. 10. Wind disturbance and mission flags.

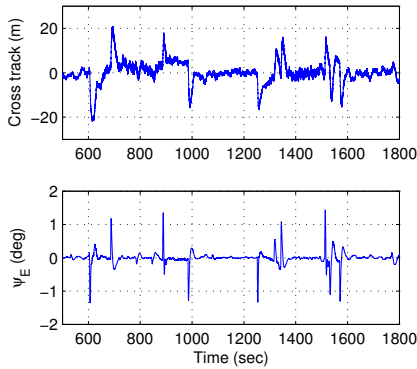


Fig. 11. Cross-track error and heading error (ψ_E).

is presented. The methodology has been developed keeping in view the practical aspects of the problem and implementation on a real-time platform. Nonlinear simulation shows very encouraging results; the design is planned to be taken to flight testing shortly.

REFERENCES

J.H. Mathews. *Numerical Methods for Mathematics, Science, and Engineering*. Prentice-Hall, Englewood Cliffs, NJ, USA, second edition, 1992.

D. McFarlane and K. Glover. A loop shaping design procedure using H_∞ synthesis. *IEEE Transactions on Automatic Control*, 37(6):759–769, 1992.

D.C. McFarlane and K. Glover. *Robust Controller Design Using Normalized Coprime Factor Plant Descriptions*,

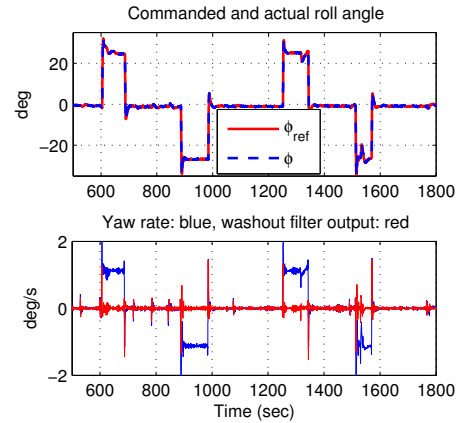


Fig. 12. Commanded and actual roll angles and yaw-rate.

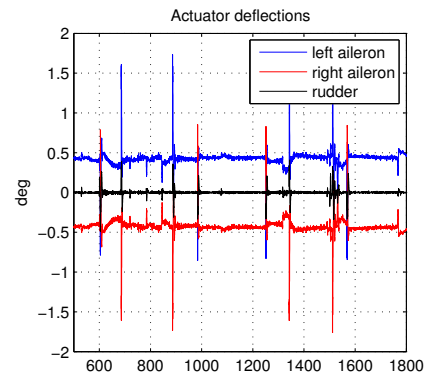


Fig. 13. Actuator deflection commands.

volume 138 of *Lecture Notes in Control and Information Sciences*. Springer-Verlag, Berlin, 1990.

S. Park, J. Deyst, and J.P. How. A new nonlinear guidance logic for trajectory tracking. In *AIAA Guidance, Navigation, and Control Conference and Exhibit*, Providence, Rhode Island, 16-19 August 2004.

I. Postlethwaite, E. Prempain, E. Turkoglu, M.C. Turner, K. Ellis, and A.W. Gubbells. Design and flight testing of various H_∞ controllers for the Bell 205 helicopter. *Control Engineering Practice*, 13:383–398, 2005.

R. Samar, G. Murad, I. Postlethwaite, and D.-W. Gu. A discrete time H_∞ observer-based controller and its application to a glass tube production process. *European Journal of Control*, 2:112–125, 1996.

R. Samar, S. Ahmed, and M.F. Aftab. Lateral control with improved performance for UAVs. In *17th IFAC Symposium on Automatic Control in Aerospace*, Toulouse, France, 2007.

S. Skogestad and I. Postlethwaite. *Multivariable Feedback Control Analysis and Design*. John Wiley & Sons, West Sussex, England, second edition, 2005.

A. Smerlas, D.J. Walker, I. Postlethwaite, M.E. Strange, J. Howitt, and A.W. Gubbells. Evaluating H_∞ controllers on the NRC Bell 205 fly-by-wire helicopter. *Control Engineering Practice*, 9(1):1–10, 2001.

M.C. Tsai, E.J.M. Geddes, and I. Postlethwaite. Pole-zero cancellations and closed-loop properties of an H_∞ mixed sensitivity design problem. *Automatica*, 28(3):519–530, 1992.